Journal of Materials Chemistry A

ROYAL SOCIETY OF CHEMISTRY

PAPER

View Article Online
View Journal | View Issue

Cite this: J. Mater. Chem. A, 2025, 13, 35575

Shape memory alloy-reinforced self-healing aluminum composites with *in situ* low melting point healing phase

Masum Bellah, [a] Vaibhav Srivastava, [b] Michael Nosonovsky, *[a] Benjamin Church [b] and Pradeep Rohatgi[ab]

Received 29th June 2025
Accepted 11th September 2025

DOI: 10.1039/d5ta05255f

rsc.li/materials-a

Shape memory alloy (SMA)-reinforced self-healing metal matrix composites (SHMMCs) are an emerging class of materials capable of semi-autonomously repairing cracks—a process termed assisted self-healing, offering significant potential for enhancing structural longevity. This study investigated the effects of varying SMA volume fractions (1.5 and 4.2 vol%) and *in situ* low melting point phases (15 and 40 wt% tin) on the self-healing performance of the aluminum matrix composites. Additionally, the study investigates the influence of a clamping mechanism and the use of etchants and a phosphoric acid-based flux on enhancing load transfer and improving healing efficiency in NiTi SMA-reinforced SHMMCs. Flexural testing confirmed the restoration of mechanical properties after healing, while microstructural characterization using Scanning Electron Microscopy (SEM) and Energy Dispersive Spectroscopy Analysis (EDS) revealed interfacial bonding between the Al–Sn matrix and NiTi reinforcement. Among the tested compositions, the Al–40 wt% Sn–1.5 vol% NiTi composite without a clamping mechanism exhibits the highest flexural property recovery, attributed to the synergistic effect of shape restoration by the NiTi SMA and effective sealing of the healing agent at the crack site. These findings highlight the potential of SMA-reinforced SHMMCs for enhancing material durability and sustainability.

1. Introduction

Among various self-healing metallic material concepts, Shape Memory Alloy (SMA)-reinforced Self-Healing Metal Matrix Composites (SHMMCs) have emerged as one of the most studied and promising systems at the macroscale.[1–5] These composites utilize the unique properties of SMAs, particularly their ability to generate shrinkage and compressive stresses during phase transformation, which aids in crack closure and facilitates healing.[4,6–12] In NiTi, this capability arises from the shape memory effect—a reversible martensitic transformation involving the B19′ (monoclinic) and, in some compositions or thermomechanical states, the B19 (orthorhombic) martensites; upon heating above A_f, both B19′ and B19 transform back to B2 (austenite), producing recovery strain/stress that clamps and narrows cracks.[13–16] To enhance self-healing efficiency, matrix alloys incorporating low-melting-point eutectic phases have been explored, since they enable localized liquefaction and flow of the low-melting healing phase to the crack site at an appropriate healing temperature and seal the crack.[6,7,17–28] Operationally, damage induced by tensile or flexural stresses, stretches the embedded SMA fibers, subsequent heating activates recovery stress in the SMA fibers and the eutectic phase partially melts and fills the crack, sealing the crack on solidification.[4] In the past, various alloy systems have been used as matrix materials in SHMMCs, including Sn–13 at% Bi,[7] Mg–5.7 at% Zn–2.7 at% Al,[7] Al–4.5 at% Cu,[23] Al–4.1 at% Cu–2.0 at% Si,[23] Al–3 at% Si,[21] Sn–20 wt% Bi,[29,30] Sn–13 wt% Bi,[31] Bi–10 wt% Sn,[29] Zn–0.8Al–0.015Cu,[32] and AA2014.[33–38]

Manuel *et al.*[6,7] synthesized SMA-reinforced SHMMCs using Sn–Bi and Mg–Zn–Al matrices with ~1 vol% continuous NiTi wires, achieving near-full tensile strength recovery in Sn–Bi but only partial closure of crack in the stronger Mg alloy where SMA force was insufficient to close rough crack surfaces. Misra *et al.*[1,29,30] employed pressure-infiltrated Sn–Bi/Bi–Sn matrices with ~20 vol% NiTi to obtain complete crack closure, full shape recovery, and high flexural strength recovery (92% for Sn–20% Bi–NiTi and 88% for Bi–10% Sn–NiTi). Wright *et al.*[20] demonstrated that microstructure and matrix ductility govern healing efficiency: Al–Si/NiTi composites retained ~90% UTS after healing, whereas Al–Cu-based systems showed little healing due to insufficient ductility of the matrix preventing effective SMA transformation. Fisher *et al.*[17,23] embedded 2 vol% NiTi in Al–Si and reported ~92% tensile healing efficiency, with evidence of fatigue-crack healing. Poormir *et al.*[24,31] and Srivastava *et al.* showed[33–39] that SMA volume fraction, pre-strain, healing temperature, healing time, and solder reservoirs all play

[a]Department of Mechanical Engineering, University of Wisconsin - Milwaukee, Milwaukee, WI 53211, USA. E-mail: nosonovs@uwm.edu

[b]Department of Materials Science and Engineering, University of Wisconsin - Milwaukee, Milwaukee, WI 53211, USA

important roles in self-healing. Sharma *et al.*[40,41] demonstrated that in semi-solid processed composites partial crack closure occurs in short times. Zhu *et al.*[18,28] confirmed through modeling that pre-strain and matrix softening are important for healing. Manuel *et al.*[22] proposed that negative-CTE reinforcements could be used as an alternative to SMA. Tasan *et al.*[5] suggested that SMA nanoparticles might enable autonomous nanoscale healing, but this has not yet been experimentally verified.

An alternative approach to healing involves *ex situ* healing agents encapsulated in tubes, capsules, or microballoons, which release low-melting-point healing liquids such as Sn, In, Zn, Sn–Bi, Sn–Pb, or Zn–Al upon rupture at healing temperature.[42–48] These healing agents are incorporated into metal matrices (*e.g.*, Al, Al206, Al5083, Sn, or Sn–Cu alloys) *via* conventional solidification techniques[42–48] or, more recently, through additive manufacturing.[49] These studies did not report recovery of mechanical properties during healing. Moreover, this method faces several challenges, including difficulties in uniformly embedding the capsules, as well as issues related to surface tension, capillarity, and viscous resistance, which hinder the healing liquid from entering cracks, forming effective bonds, and achieving reliable healing. Since the healing process depends on the rupture of encapsulated agents, cracks occurring in regions without capsules remain unhealed, resulting in inconsistent and location-dependent performance. Additionally, voids left after agent release can compromise mechanical integrity. These systems are typically limited to single-cycle healing, as once the agent solidifies within a crack, the original capsule sites remain voided, reducing structural strength and precluding further healing without additional processing.[50]

To address these limitations, *in situ* low-melting-point phase-based SMA-reinforced SHMMCs offer an advanced approach to self-healing. In these systems, the low melting point phase is formed or retained within the matrix during fabrication, similar to metallic composite phase change materials,[51–54] thereby eliminating the need for externally encapsulated healing agents. This enhances the scalability and practicality of the self-healing mechanism. The embedded *in situ* low-melting-point phase acts as a healing agent, melting at a temperature lower than that of the matrix, flowing into cracks, and subsequently solidifying to restore structural integrity. Unlike eutectic-based self-healing, the healing process in this system occurs at substantially lower temperatures. The use of an *in situ* low-melting-point phase is particularly advantageous, enabling healing with reduced thermal input. This promotes energy conservation during the healing cycle and facilitates the potential application of novel techniques, such as electro-healing, to repair the composites. Designing the composite microstructure to optimize the flow of this healing phase is crucial to achieving efficient crack filling and strength recovery.

Previous research by Jeong *et al.*[52] demonstrated self-healing capabilities in $(Al_{81}Cu_{13}Si_6)_{100-x}(Sn_{57}Bi_{43})_x$ (x = 1 and 3 at%) composites, where dual self-healing properties were observed through precipitate formation and *in situ* low-melting-temperature metallic healing agents. However, these composites did not incorporate SMA reinforcements. By integrating SMA within a matrix containing an *in situ* low melting point phase, it is possible to leverage the shape memory effect for enhanced healing efficiency. The compressive force exerted by the SMA during phase transformation reduces crack size, facilitating the filling of smaller cracks compared to macro-scale defects. This synergistic approach holds significant promise for improving self-healing efficiency and mechanical performance in SHMMCs.

In this study, the design, synthesis, and self-healing performance of SMA-reinforced aluminum–tin (Al–Sn) matrix composites are investigated, with tin functioning as an *in situ* low-melting-point healing phase (melting at 228 °C). The key self-healing mechanisms—including crack narrowing and closure, strength, modulus, toughness recovery, and shape restoration—are analyzed and experimentally validated. A comprehensive microstructural analysis of the self-healing Al–Sn composites is conducted, with particular focus on interfacial bonding between the NiTi fibers and the matrix. Additionally, the effects of a mechanical clamping system for securing the NiTi SMA wires, as well as the use of etchants and phosphoric acid-based flux to enhance bonding and improve healing efficiency, are investigated. The influence of different SMA volume fractions (1.5 and 4.2 vol%) and *in situ* low-melting-point phase contents (15 and 40 wt% Sn) on self-healing performance is systematically evaluated. Bending tests are performed to assess crack closure, flexural property recovery, and shape restoration, ensuring that the induced strain remains within the elastic range of the SMA to maximize recovery. By integrating SMAs with *in situ* low-melting-point healing phases, this research advances the development of next-generation self-healing metallic materials, offering enhanced durability, repairability, and energy efficiency for structural applications.

2. Experimental section

The experimental procedure is described as follows. NiTi SMA-reinforced self-healing Al–Sn composites were synthesized using permanent steel mold die casting. Differential Scanning Calorimetry (DSC) (TA Instruments Q200) tests were conducted to determine the transformation temperatures of the NiTi SMA and the Al–Sn composition used as matrix materials. Microstructural analysis was performed using Scanning Electron Microscopy (SEM) and Energy Dispersive Spectroscopy (EDS) (JEOL 6460LV) to evaluate the effects of etching and fluxing on interfacial bonding, as well as to examine the distribution of the *in situ* low melting point phase within the microstructure. A three-point bend test was performed on the specimens using an Instron 5980 universal testing machine with a 250 kN capacity to induce controlled surface cracks. Flexural test specimens were prepared according to ASTM E290 standards for the three-point bending test.[55] Since Al–Sn is a ductile material, inducing cracks through tensile testing poses a high risk of causing plastic deformation in the SMA wires. To mitigate this, a bending test with a predefined crack path was employed in this study instead of tensile testing to generate the crack in the fabricated samples. A 0.75 mm deep, 45° notch was machined

at the center of each specimen to ensure consistent crack formation. Preventing permanent strains in SMA wires is critical, as such deformation can impair shape recovery and hinder crack closure. Bending tests further enable simultaneous evaluation of shape restoration, crack narrowing, and closure behavior, enabled by SMA reinforcement. Healing experiments were conducted in an inert atmosphere using a custom-designed box furnace (Thermo Scientific Thermolyne Small Benchtop Muffle Furnace with A1 Controller, 1.3 L, 120 V).

2.1 Materials

NiTi wire (0.51 mm diameter) was purchased from Dynalloy, Inc. Pure aluminum (99.8% purity) and pure tin (99.9% purity) were purchased from RotoMetals. Hydrofluoric acid (ACS reagent, 48%) and nitric acid (ACS reagent, 70%) were purchased from Millipore Sigma. Indalloy Flux #2 was purchased from the Indium Corporation of America. Stainless steel threaded rods were purchased from Speedy Metals, New Berlin.

2.2 Synthesis of self-healing aluminum composites with *in situ* low melting point phase

A permanent mold die was designed to cast self-healing aluminum composite samples with an *in situ* low-melting-point phase, with or without a clamping mechanism, as shown in Fig. 1(a). To improve the bonding between the NiTi wires and the matrix material, the wires underwent a surface preparation process consisting of etching and fluxing, as detailed below:

- The wires were first immersed in an aqueous solution containing 4.8% HF and 10.5% HNO_3 for 5 minutes to etch the surface.
- To remove residual flux, the etched wires were sequentially rinsed in two HDPE bottles filled with distilled water for 30 minutes and 15 minutes, respectively.

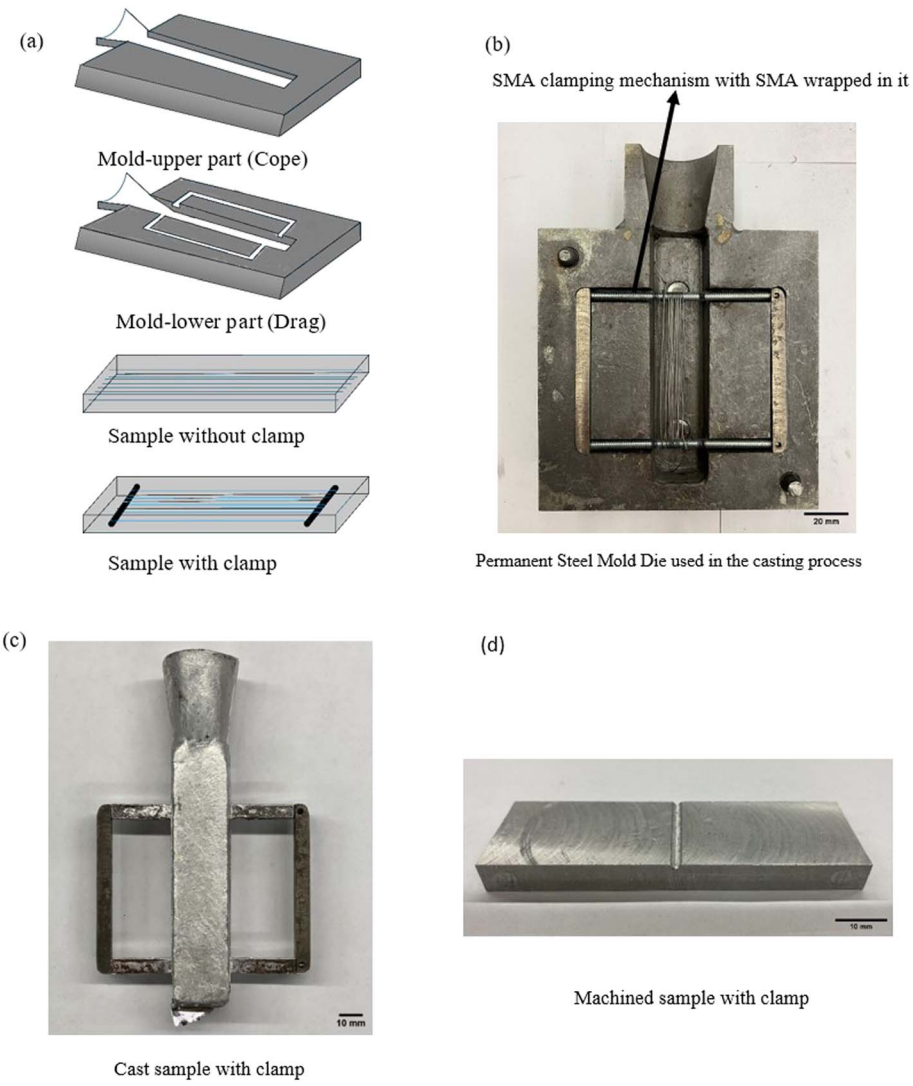

Fig. 1 (a) Mold and sample design for casting self-healing aluminum composites with *in situ* low-melting-point phase; (b) permanent steel mold die used in the casting process; (c) cast sample with clamping mechanism; (d) machined sample with clamping mechanism.

Table 1 Identification of synthesized samples

Sample id	Sn (wt%)	NiTi (vol%)	Dimensions ($l \times b \times h$) (mm^3)	Clamping mechanism
Al15Sn4.2NiTiWC	15	4.2	60 × 23 × 7	No
Al15Sn4.2NiTi	15	4.2	78 × 23.5 × 9	Yes
Al40Sn1.5NiTi	40	1.5	77 × 23 × 7	Yes
Al40Sn1.5NiTiWC	40	1.5	60 × 23 × 7	No

• Following rinsing, the wires were treated (pickled) in a phosphoric acid-based commercial flux, Indalloy Flux #2 (Indium Corporation of America), for 3 minutes.

• After fluxing, the wires were placed in an empty HDPE bottle for 30 minutes to dry and stabilize the treated surface.

The etched and fluxed NiTi wires were then wrapped around the SMA clamping mechanism, as shown in Fig. 1(b). Permanent mold gravity die casting was used to fabricate the samples. A suitable amount of aluminum (purity 99.8%) and tin (purity 99.9%) was melted in a graphite crucible using a TOAUTO 3KG Gold Melting Furnace (TGF3000, 1400 W, 2000 °F Digital Electric Melting Furnace) at 750 °C. The Al–Sn melt was then poured over the NiTi wires (50–50 at% from Dynalloy) and allowed to cool. The cast sample with the clamping mechanism is shown in Fig. 1(c). After casting, the samples were machined to the dimensions provided in Table 1. Fig. 1(d) shows the machined sample with the clamping mechanism.

The identification of the synthesized samples is provided in Table 1.

2.3 Healing of samples in self-healing aluminum composites with *in situ* low melting point phase

Samples were healed in an inert gas environment in a custom-designed box furnace (Thermo Scientific Thermolyne Small Benchtop Muffle Furnace with A1 Controller, 1.3 L, 120 V), as shown in Fig. S1 (SI). The samples were heated to 300 °C and maintained at this temperature for 1 hour to simultaneously activate the SMA wires and melt the *in situ* low-melting-point phase. The *in situ* tin is expected to melt at 228 °C, as shown in Fig. S2 of the Al–Sn phase diagram. Heating to 300 °C was intended to promote crack narrowing through SMA-induced compressive stresses and to enhance the flow of the molten phase for effective crack filling. Shape restoration and progressive crack closure were observed during the healing process. Previous studies[29,36] have shown that shape recovery rates in NiTi are maximized within several minutes once the temperature exceeds the austenite finish temperature; however, the kinetics depend on factors such as sample size, NiTi volume fraction, recovery stress generation capability, and the softening behavior of the surrounding matrix. Extending the healing duration beyond 1 hour is not very likely to further improve recovery, and excessive times may even be detrimental due to potential microstructural coarsening and oxidation in ambient atmospheres. Therefore, while the chosen temperature of 300 °C for 1 hour was effective in the present study, more systematic studies are needed to fully establish the healing kinetics and optimize duration of healing at different temperatures for different compositions and geometries.

3. Results and discussions

The relationship between eutectic/*in situ* low-melting-point phase composition and healing efficiency is not yet fully understood in higher-strength matrix alloy systems. The volume fraction of SMA wires and the *in situ* low-melting-point phase are critical factors influencing healing efficiency. This study systematically investigated how variations in these parameters affect self-healing behavior. Effective load transfer is essential for the self-healing of SMA-reinforced Al–Sn composites. To ensure strong bonding with the matrix material and facilitate efficient load transfer, the SMA wires were etched and flux-treated. Additionally, a clamping mechanism was employed, and its effect on self-healing was assessed by preparing samples with and without clamping.

Samples containing 15 wt% Sn were reinforced with a higher volume fraction of SMA wires to promote effective crack closure, thereby allowing the low-melting-point phase to fill and seal the cracks. Conversely, samples with 40 wt% Sn incorporated a lower SMA volume fraction. This approach ensures that a sufficient quantity of liquid phase remains available to accommodate larger crack openings during healing. Tin was chosen as the *in situ* low-melting-point phase because of its relatively low melting temperature compared to conventional eutectic phase-based aluminum alloys. Fig. S3 presents the DSC analysis of Al–15 wt% Sn, Al–40 wt% Sn, and NiTi. The DSC results for NiTi reveal an austenite start temperature of 59.8 °C and a finish temperature of 77.3 °C, with martensite start and finish temperatures of 61.3 °C and 45.9 °C, respectively. These findings confirm that NiTi exhibits the reversible phase transformations required for healing. Upon crack formation, twinned martensite transitions to detwinned martensite. Heating initiates a transformation to austenite, and subsequent cooling restores the original twinned martensite structure, aiding shape and crack closure recovery. The DSC curves for Al–15 wt% Sn and Al–40 wt% Sn indicate tin-rich liquid phase melting at 230.4 °C and 233.4 °C, respectively, confirming the availability of a liquid healing phase. The larger integrated area of the melting peak observed in Al–40 wt% Sn indicates a higher fraction of molten Sn-phase, which may enhance healing efficiency. SEM and EDS characterization of Al–15 wt% Sn–NiTi and Al–40 wt% Sn–NiTi composites verified the elemental composition of both matrix and reinforcement. Tin enrichment at grain boundaries was observed (Fig. S4–S7), with tin content

increasing progressively from ~10 wt% in Al–15 wt% Sn to ~40 wt% in Al–40 wt% Sn. The presence of tin at grain boundaries is associated with improved ductility of the composites. To further quantify the distribution of tin within the matrix, EDS area analysis was carried out on multiple regions of the Al–15 wt% Sn and Al–40 wt% Sn composites. For Al–15 wt% Sn, the Sn concentration averaged ~10.5 wt% with a narrow standard deviation of 0.93 wt% (Fig. S8). In the Al–40 wt% Sn composite, the Sn concentration averaged ~33.6 wt% with a slightly higher standard deviation of 5.85 wt% (Fig. S9). Overall, the distribution of Sn in both compositions is macroscopically uniform across the matrix. Lower than expected Sn levels can be due to the use of standardless quantification routines in the software and the nature of EDS quantification difficulties when the sample contains elements of vastly different atomic weights such as is the case with Al and Sn.[56]

Surface treatment of NiTi wires through etching and fluxing produced a roughened surface morphology, as shown in Fig. S10, which enhances mechanical interlocking with the matrix, promoting efficient load transfer and improved healing performance. In addition, fluxing treatment also improves interfacial wettability by dissolving the native oxide layer on NiTi and increasing the surface energy, which promotes better spreading of the molten Al–Sn phase on the reinforcement.[29,57–60] Enhanced wetting between the NiTi fiber and Al–Sn matrix and mechanical interlocking between the roughened surface of the fiber and the matrix led to load transfer between the NiTi fibers and the matrix and the fiber pullout is prevented. Between Al–15 wt% Sn and NiTi, the aluminum–tin alloy (whether Al–15 wt% Sn or Al–40 wt% Sn) has a higher thermal coefficient of expansion (CTE). Al–15 wt% Sn has a CTE of approximately 23–25 $\times$ 10^{-6}/°C, while Al–40 wt% Sn can be estimated to be in the range of 25–27 $\times$ 10^{-6}/°C.[61,62] In contrast, NiTi has a CTE of approximately 11–12 $\times$ 10^{-6}/°C in the austenite phase and 6–8 $\times$ 10^{-6}/°C in the martensite phase.[63] This difference in CTE causes the matrix in the composite to shrink radially more than the fiber upon cooling from a high temperature. Good contact between the

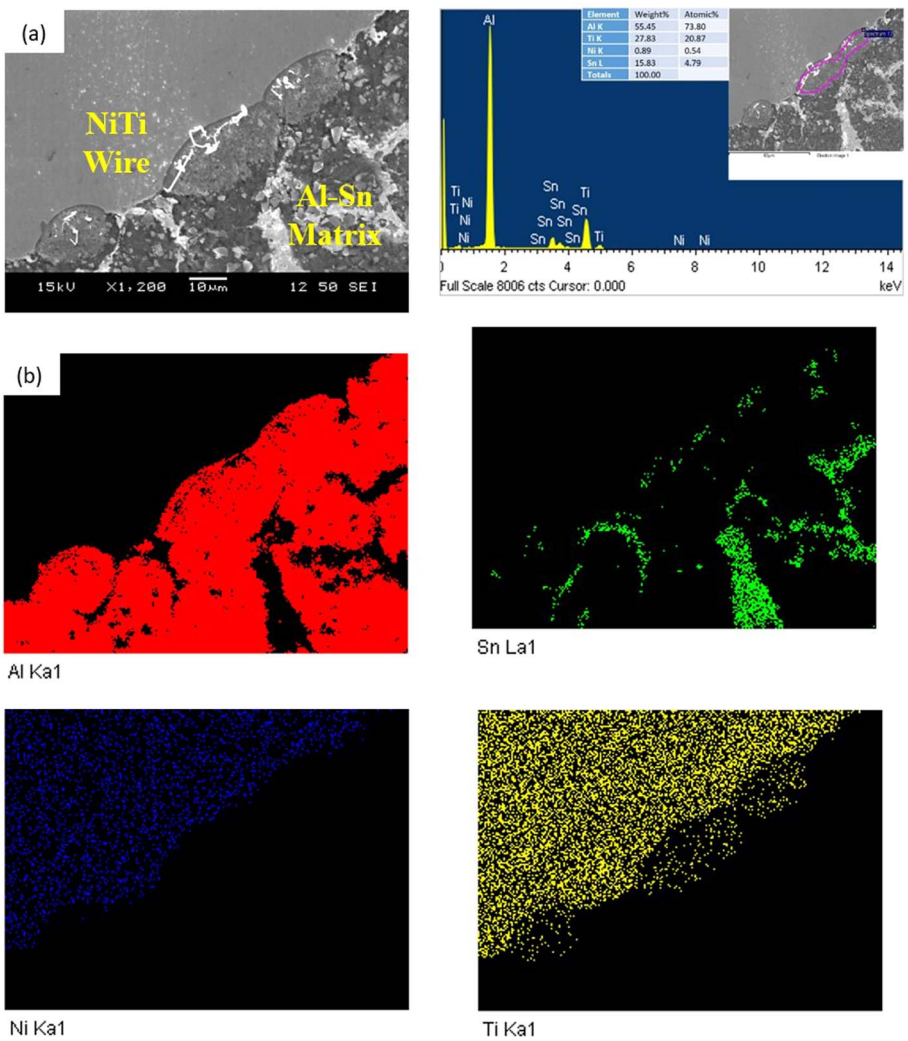

Fig. 2 (a) The results of the EDS analysis indicate that a chemical reaction has occurred in the interface, resulting in a chemical composition of Al, Sn, Ni, and Ti. (b) EDS elemental mapping confirms the interfacial reaction, showing a chemical composition comprising Al, Sn, Ni, and Ti.

NiTi and the matrix is observed, as shown in Fig. S4–S7 and 2. Effective mechanical bonding requires that the matrix fill the hills and valleys on the surface of the reinforcement and this is facilitated by good wetting. Furthermore, some reaction bonding also occurs at the interface, as demonstrated in Fig. 2. The reaction zone, consisting of Al, Sn, Ni, and Ti, indicates transport of atoms and their reaction at the interface. Fig. 2 illustrates how the asperities in the NiTi are filled by the matrix, along with evidence of chemical reactions at the interface. The combined effects of mechanical interlocking and reaction bonding contribute to the overall bond strength. Achieving optimal bonding facilitates efficient load transfer between the matrix and reinforcement and improves healing efficiency. Collectively, the rough topography, thin reaction interlayer, and CTE-induced shrink-fit are consistent with a shear-lag load-transfer mechanism that suppresses interfacial slip. During healing, the same bonded, well-wetted interface efficiently transmits NiTi recovery stresses to deform the matrix and narrow and close the crack.

The healing efficiency of the SHMMC is assessed by comparing the flexural properties (FP) of the virgin composite with the post-healing flexural properties of the same composite, using eqn (1):

$$\frac{FP_{healed}}{FP_{virgin}} \times 100\% = \%\ \text{recovery} \quad (1)$$

The flexural stress *vs.* strain graph for the self-healing aluminum–tin composite samples is depicted in Fig. 3, and the results are presented in Table 2. Among all the tested samples, the Al40Sn1.5NiTi exhibited the highest flexural strength. The inclusion of a clamping mechanism enhanced the strength of the samples for both the Al–40 wt% Sn and Al–15 wt% Sn matrix materials. Furthermore, the addition of tin to aluminum improved the flexural toughness of the samples. Fig. 4(a) and (b) show the flexural strength and specific flexural strength of the intact and healed composite samples with varying tin content, NiTi volume fractions, and the presence or absence of a clamping mechanism, while Table 2 presents their flexural strength recovery and specific flexural strength recovery, respectively. The flexural strength recovery of the SMA-reinforced self-healing aluminum–tin composites provides insight into the effectiveness of the self-healing mechanism. Among the four tested samples, the Al40Sn1.5NiTiWC composite (40 wt% Sn, 1.5 vol% NiTi, without clamping) exhibited the highest flexural strength recovery (90%), demonstrating the advantage of incorporating a high Sn content in the matrix. The enhanced healing efficiency can be attributed to the greater availability of the low-melting-point Sn phase, which effectively filled and sealed the cracks upon heating. Conversely, the Al15Sn4.2NiTi composite (15 wt% Sn, 4.2 vol% NiTi, with clamping) exhibited the lowest strength recovery (44.58%), highlighting the potential limitations of using a lower Sn content combined with a higher NiTi volume fraction. This suggests that, while the shape memory effect of NiTi contributes to crack closure, the absence of sufficient healing liquid from Sn may hinder complete crack filling and sealing, ultimately affecting the strength recovery. Moreover, while the clamping mechanism improved the initial intact flexural strength of the samples, it had a negative impact on healing efficiency due to the introduction of a weak point in the structure, where Sn may have preferentially flowed, thereby reducing the effectiveness of the healing process.

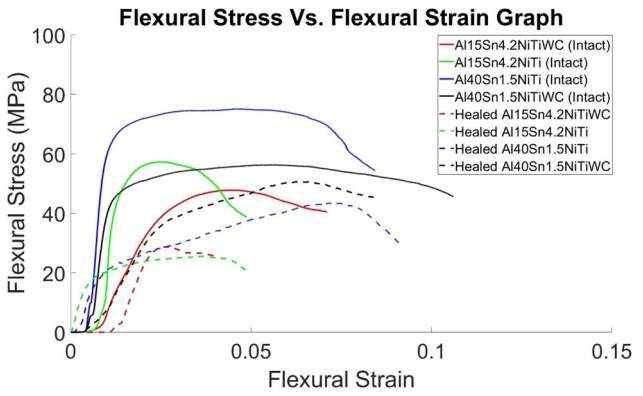

Fig. 3 Flexural stress *vs.* strain graph of fabricated samples of self-healing aluminum composites.

Fig. 4(c) and (d) show the flexural modulus and specific flexural modulus of the intact and healed composite samples with varying tin content, NiTi volume fractions, and the presence or absence of a clamping mechanism, while Table 3 presents their flexural modulus recovery and specific flexural modulus recovery, respectively. The flexural modulus and specific flexural modulus recovery results indicate that, while healing restored strength to some extent, the stiffness of the material was significantly reduced after healing. This suggests microstructural changes that impact the load-bearing capability

Table 2 Flexural strength and specific flexural strength recovery of fabricated samples of SMA-reinforced self-healing aluminum–tin composites

	Flexural strength		Specific flexural strength		
Sample id	Intact sample (MPa)	Healed sample (MPa)	Intact sample (10^3 N m kg^{-1})	Healed sample (10^3 N m kg^{-1})	% Strength and specific flexural strength recovery
Al15Sn4.2NiTiWC	47.8	28.7	12.9	7.74	60
Al15Sn4.2NiTi	57.26	25.53	17.7	7.9	44.6
Al40Sn1.5NiTi	75.15	43.43	21.1	12.2	57.8
Al40Sn1.5NiTiWC	56.3	50.7	14.9	13.4	90

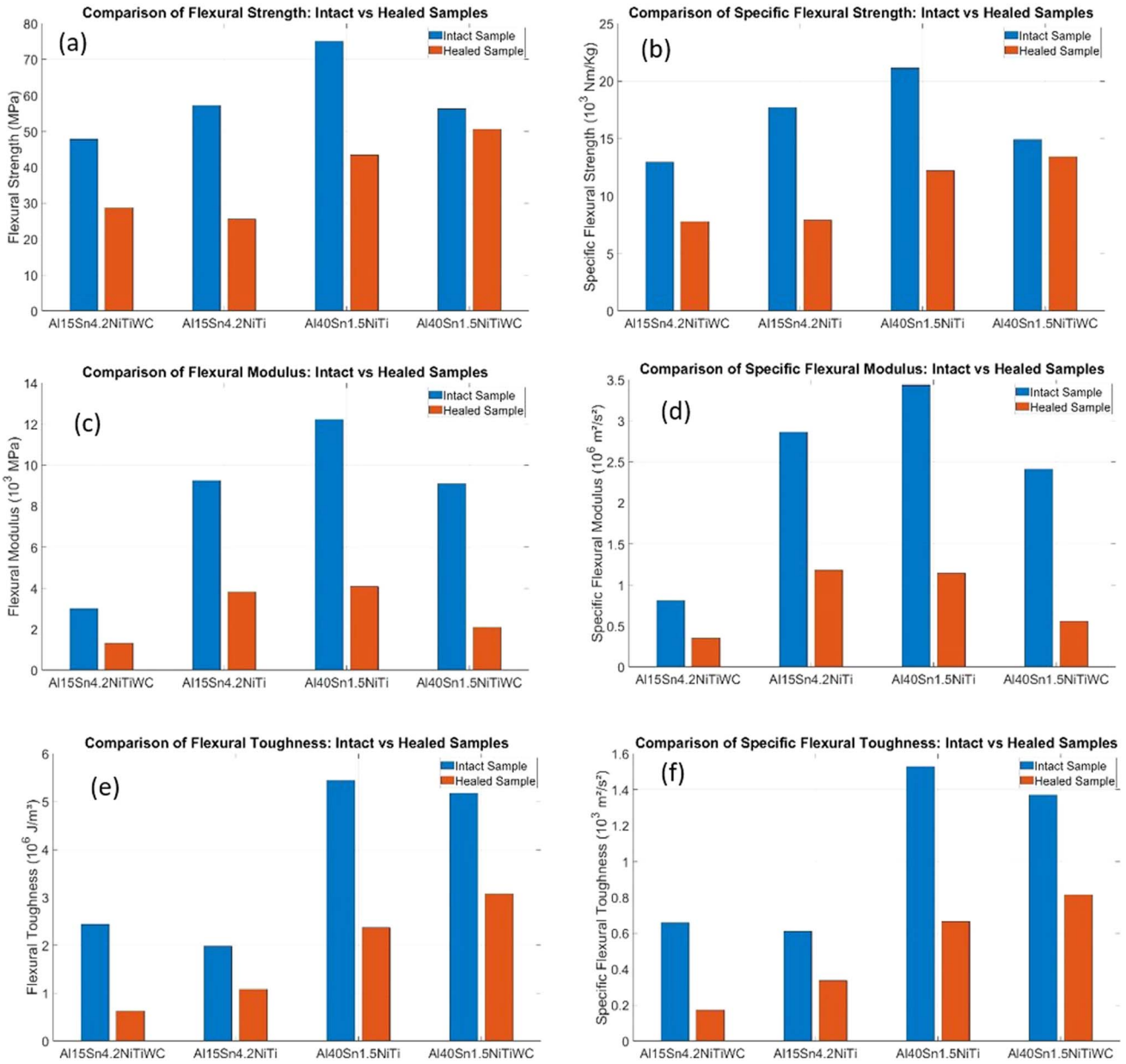

Fig. 4 (a) Flexural strength (b) specific flexural strength (c) flexural modulus (d) specific flexural modulus (e) flexural toughness (f) specific flexural toughness of the intact and healed composite samples with varying tin content, NiTi volume fractions, and the presence or absence of a clamping mechanism.

of the composite post-healing. The highest flexural modulus and specific flexural modulus recovery were observed in the Al15Sn4.2NiTiWC composite (43.3%), indicating that a lower Sn content and absence of clamping helped retain structural stiffness after healing. Conversely, the Al40Sn1.5NiTiWC composite exhibited the lowest flexural modulus and specific flexural modulus recovery (23.1%), suggesting that while a higher Sn content improves crack sealing and strength recovery, it reduces stiffness post-healing. This may be due to the redistribution of the Sn phase after healing, leading to localized softening in the matrix. Overall, increasing the NiTi volume fraction led to improved flexural modulus and specific flexural modulus recovery. These findings imply that, while a higher Sn fraction enhances healing efficiency in terms of strength recovery, it introduces a trade-off in terms of stiffness loss.

Fig. 4(e) and (f) show the flexural toughness and specific flexural toughness of the intact and healed composite samples with varying tin content, NiTi volume fractions, and the presence or absence of a clamping mechanism, while Table 4 presents their flexural toughness recovery and specific flexural toughness recovery, respectively. The analysis of flexural toughness recovery provides critical insights into the damage tolerance and energy absorption capacity of the healed samples. The Al40Sn1.5NiTiWC composite demonstrated the highest flexural toughness and specific flexural toughness recovery

Table 3 Flexural modulus and specific flexural modulus recovery of fabricated SMA-reinforced self-healing aluminum–tin composites

	Flexural modulus		Specific flexural modulus		
Sample id	Intact sample (10^3 MPa)	Healed sample (10^3 MPa)	Intact sample (10^6 m^2 s^{-2})	Healed sample (10^6 m^2 s^{-2})	% Flexural modulus and specific flexural modulus recovery
Al15Sn4.2NiTiWC	3	1.3	0.81	0.35	43.3
Al15Sn4.2NiTi	9.3	3.8	2.9	1.18	40.8
Al40Sn1.5NiTi	12.2	4	3.4	1.12	32.8
Al40Sn1.5NiTiWC	9.1	2.1	2.4	0.56	23.1

Table 4 Flexural toughness recovery of fabricated SMA-reinforced self-healing aluminum–tin composites

	Flexural toughness		Specific flexural toughness		
Sample id	Intact sample (10^6 J m^{-3})	Healed sample (10^6 J m^{-3})	Intact sample (10^3 m^2 s^{-2})	Healed sample (10^3 m^2 s^{-2})	% Flexural toughness and specific flexural toughness recovery
Al15Sn4.2NiTiWC	2.4	0.64	0.66	0.17	26.7
Al15Sn4.2NiTi	1.98	1.08	0.61	0.34	54.5
Al40Sn1.5NiTi	5.4	2.37	1.53	0.67	43.9
Al40Sn1.5NiTiWC	5.2	3.08	1.37	0.82	59.2

(59.2%), highlighting that a higher Sn content facilitates a more effective crack-sealing process. The ability of the Sn phase to flow into cracks and resolidify plays a crucial role in restoring the material's resistance to fracture. In contrast, the Al15Sn4.2NiTiWC composite exhibited the lowest toughness recovery (26.7%), suggesting that a lower Sn content may not provide sufficient healing liquid to fill and seal cracks effectively, leading to a lower degree of toughness restoration. Interestingly, the toughness recovery was higher in the Al40Sn1.5NiTi samples compared to the Al15Sn4.2NiTi samples, reinforcing the hypothesis that increasing the *in situ* low melting point phase contributes positively to damage recovery.

The clamping mechanism was introduced to improve load transfer between the NiTi wires and the aluminum matrix. While clamping enhanced the initial intact strength of the composite by reinforcing the material structure, the presence of a clamping reduced flexural strength recovery. Fig. S11(a) shows an optical image of the area near the clamp before healing, and Fig. S11(b) shows the corresponding area after healing, where Sn-rich healing agent is visible around the clamp. Fig. S11(c) presents a microstructural SEM image of the clamp region before healing, while Fig. S11(d) shows the microstructural SEM image after healing along with EDS analysis of the healing agent. These results indicate that although clamping improves mechanical integrity before damage occurs, there was seeping of tin around the clamping bar, and this may have an effect of the strength of the healed sample. More systematic studies are needed to understand the effect of clamping on recovery of strength on healing.

The crack area of the samples was measured before and after healing using ImageJ software. For Al15Sn4.2NiTiWC, the crack area before healing was found to be 6.8 mm^2. After healing, the crack area was reduced to 3 mm^2, resulting in a percentage reduction of 55.9%, as shown in Fig. S12. The percentage reduction in crack area is calculated using the following eqn (2):

$$\frac{\text{Crack area before healing} - \text{crack area after healing}}{\text{Crack area before healing}} \times 100\% = \%\ \text{reduction in crack area} \quad (2)$$

For Al15Sn4.2NiTi, the crack area before healing was 16.3 mm^2, and after healing, it was reduced to 9.7 mm^2, yielding a percentage reduction of 40.5%, as shown in Fig. S13. For Al40Sn1.5NiTi, the crack area before healing was 27.3 mm^2, and after healing, it was reduced to 5.2 mm^2, resulting in a percentage reduction of 81%, as shown in Fig. 5. For Al40Sn1.5NiTiWC, the crack area before healing was 19.8 mm^2, and after healing, it was reduced to 9.4 mm^2, leading to a percentage reduction of 52.5%, as shown in Fig. S14. The highest reduction in crack area was observed in sample Al40Sn1.5NiTi, which can be attributed to the synergistic effect of NiTi wire and crack sealing by the low melting point tin phase.

The analysis of crack area reduction in self-healing aluminum–tin composites reveals that a higher Sn content (40 wt%) significantly enhances crack-narrowing healing efficiency, as observed in the Al40Sn1.5NiTi sample, which exhibited the highest crack area reduction of 81%. This superior healing performance is attributed to the increased availability of low-melting-point Sn, which effectively flows into cracks and seals them upon heating, combined with matrix softening at the healing temperature. Additionally, the synergistic effect of NiTi reinforcement played a crucial role in facilitating crack closure, as the shape memory effect of NiTi induces compressive stresses that aid in the healing process. Conversely, samples with lower Sn content (15 wt%) exhibited lower healing efficiency, with Al15Sn4.2NiTi achieving only 40.5% crack area

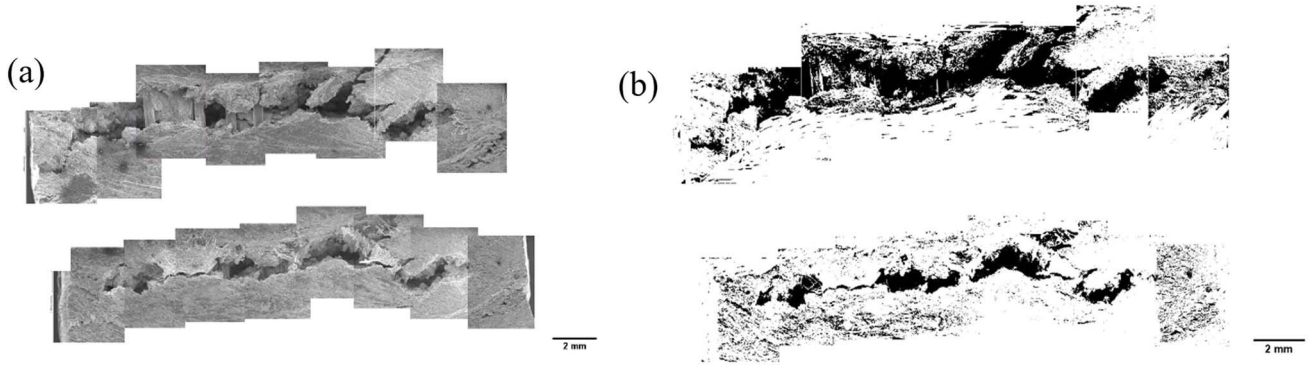

Fig. 5 (a) SEM micrograph showing the crack area before and after healing; (b) ImageJ analysis of the corresponding area. For Al40Sn1.5NiTi, the crack area before healing was measured as 27.3 mm^2, which reduced to 5.2 mm^2 after healing, resulting in a 81% reduction in the crack area (size of the scale bar: 2 mm).

reduction, indicating that insufficient healing liquid and reduced matrix softening at the healing temperature limit the crack-sealing capability. Similarly, Al15Sn4.2NiTiWC showed a 55.9% crack area reduction, reinforcing the need for an optimal Sn percentage in self-healing aluminum–tin composites.

The highest strength recovery was observed in the Al40Sn1.5NiTiWC. This significant recovery is attributed to the effective bonding of the healing agent within the crack area, as illustrated in Fig. S15. Elemental analysis of the sealing material in crack shows that it mainly consists of tin with low levels of aluminum. Evidence of some oxide was found at the crack site even though the present healing experiments were conducted in an inert atmosphere to minimize oxidation. Real service environments may expose the material to air or moisture, where extensive oxidation can possibly occur and this will need further investigation to quantify the effect of oxidation under different geometrical and environmental conditions.

The percentage of shape restoration for the healed samples was measured using the following eqn (3):

$$\frac{\text{Bend angle for healed sample}}{\text{Bend angle of the intact sample}} \times 100\% = \%\ \text{shape restoration} \quad (3)$$

The analysis of shape restoration in self-healing aluminum–tin composites (as presented in Fig. 6(a) and (b)) reveals that the Al15Sn4.2NiTiWC sample exhibited the highest percentage of shape restoration (99.9%), indicating superior shape recovery after healing. This can be attributed to its lower ductility, which results in less severe bending before failure, allowing for a greater degree of shape retention post-healing. When comparing shape restoration between Al15Sn4.2NiTi and Al40Sn1.5NiTi, it was observed that Al40Sn1.5NiTi exhibited a slightly higher total shape restoration (6.6°) compared to 4.9° for Al15Sn4.2NiTi. This trend suggests that matrix softening at the healing temperature played a role in shape recovery for Al–40 wt% Sn samples. Overall, the results indicate that higher NiTi volume fractions enhance shape recovery due to the shape memory effect, while higher Sn content influences matrix softening, leading to variations in the degree of restoration. However, the combination of NiTi reinforcement and *in situ* low-melting-point Sn phase remains essential for optimizing self-healing performance in aluminum composites.

It should be noted that the present study was restricted to a single healing cycle for each composite. Nevertheless, the design inherently offers the potential for repeated healing. The *in situ* Sn phase remains within the matrix as shown in Fig. S11 and can re-melt and resolidify during subsequent cycles, though its availability will gradually diminish as it is consumed at crack sites. The NiTi reinforcement retains its reversible phase transformation capability, but cyclic straining within the constraints of the matrix may induce fatigue and functional degradation, potentially limiting multicycle healing.[64,65] Systematic multi-cycle healing studies are required to examine the potential of multicycle healing in the composites.

In the context of phase-change material (PCM)-assisted self-healing metals, our SMA-reinforced Al–Sn/NiTi composites achieve near-complete shape restoration (up to 99.9%), high strength recovery (up to ~90%), and up to ~81% reduction in crack area after a single healing cycle. Dual *in situ* PCM designs (*e.g.*, Al–Cu–Si with Sn–Bi) demonstrate thermally/warm-rolling-assisted crack (up to ~28 μm) filling at ~150 °C, though mechanical property recovery is not quantified.[52] In a binary Al–4.28 wt% Sn alloy, annealing at 400 °C for 30 min enabled Sn-rich eutectics to fill >90% of an artificial crack (~5 μm wide, ~1.6 mm long), resulting in a >120% increase in ductility compared with pure Al.[54] A key difference is the mechanism: SMA-assisted healing not only provides active recovery stresses that clamp and narrow cracks but also enables sealing of larger cracks that would be inaccessible to PCM alone, ensuring robust shape restoration and effective post-healing load transfer. PCM-only approaches rely primarily on capillarity and diffusion and may benefit from external pressure or deformation (*e.g.*, rolling). While PCM routes can operate at lower temperatures, SMA-assisted systems combine crack-closure forces with melt-assisted sealing, offering clear advantages where shape restoration and structural recovery are critical.

The self-healing capability in Al–Sn–NiTi reinforced components will prevent catastrophic failures and extend the life and

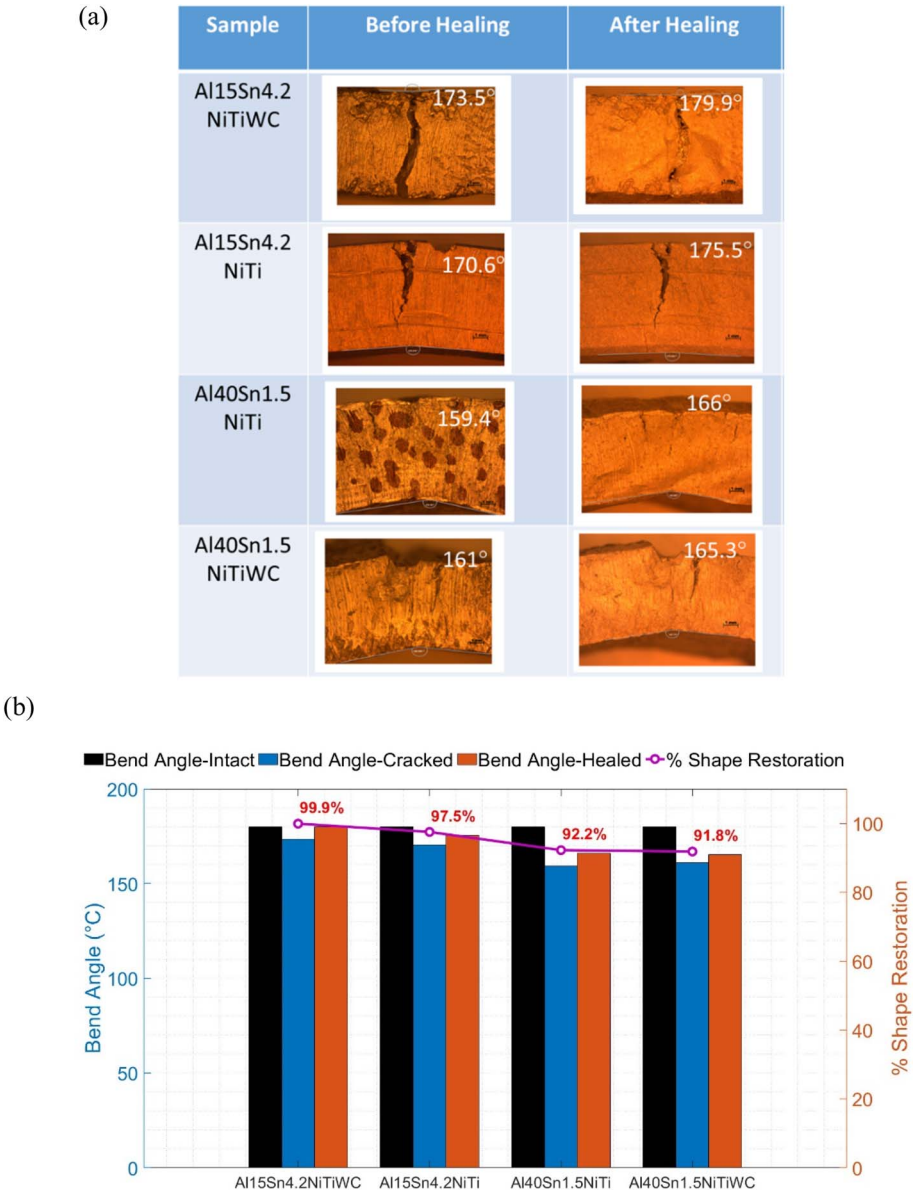

Fig. 6 Shape restoration of self-healing aluminum–tin (Al–Sn) composites: (a) optical images of samples before and after self-healing; (b) graph comparing shape restoration.

functionality, thereby reducing the need for replacement parts. This would reduce the need for materials and energy requirements to produce replacement parts and promote sustainability.

4. Conclusions

This study investigated the self-healing behavior of Shape Memory Alloy (SMA)-reinforced aluminum–tin (Al–Sn) composites with an *in situ* low melting point healing phase, focusing on crack closure, flexural property recovery, and shape restoration. The findings demonstrate that higher tin content (40 wt%) significantly enhances healing efficiency, as observed in the Al40Sn1.5NiTi composite, which exhibited the highest crack area reduction (81%) and superior strength recovery. The effectiveness of the self-healing mechanism was attributed to the synergistic effect of the NiTi SMA and *in situ* Sn phase, where the shape memory effect of NiTi assisted in crack closure while liquid tin effectively filled and sealed the cracks. The study also explored the influence of a clamping mechanism on healing efficiency. While clamping improved the initial mechanical integrity of the composite, it introduced weak points that allowed Sn to escape, reducing healing effectiveness. The highest strength recovery (90%) was observed in Al40Sn1.5NiTiWC, reinforcing the importance of matrix composition and processing conditions in self-healing performance. Additionally, shape restoration analysis revealed that higher NiTi volume fractions (4.2 vol%) contributed to better shape recovery due to the shape memory effect, whereas higher Sn content (40 wt%) led to matrix softening at the healing temperature, influencing

shape restoration. The Al15Sn4.2NiTiWC composite exhibited the highest shape restoration (99.9%), indicating that reduced ductility before failure allowed for improved post-healing shape recovery. Al40Sn1.5NiTi exhibited the actual highest total shape restoration (6.6°) among all samples. The study confirms that optimizing Sn content, NiTi reinforcement, and processing conditions is crucial for maximizing the self-healing efficiency of metal matrix composites. The results emphasize the importance of tailoring microstructural design to enhance crack healing, mechanical property retention, and shape restoration. Future research should explore alternative healing agents, different healing techniques including electro-healing, assessments of multicycle healing capabilities, and performance assessments of these composites under different loading conditions before and after healing to further enhance the practical applications of SMA-reinforced self-healing aluminum composites in structural and aerospace applications.

Author contributions

Conceptualization, M. B., V. S., M. N., and P. R.; methodology, M. B., V. S., M. N., and P. R.; software, M. B., and V. S.; validation, M. B., V. S., M. N., B. C. and P. R.; formal analysis, M. B.; investigation, M. B., and V. S.; resources, M. N., B. C. and P. R.; data curation, M. B. and V. S.; writing-original draft preparation, M. B.; writing-review and editing, M. B., V. S., M. N., B. C. and P. R.; visualization, M. B., V. S., M. N., B. C. and P. R.; supervision, M. N., B. C. and P. R.; project administration, M. B., M. N., and P. R.; funding acquisition, P. R. All authors have read and approved the final manuscript for publication.

Conflicts of interest

There is no conflict of interest.

Data availability

The data supporting the findings of this study are provided within the article and the SI. Additional data are available from the corresponding author upon reasonable request.

Supplementary information: includes an image of the box furnace used for healing; Al–Sn phase diagram; DSC curves of NiTi, Al–15 wt% Sn, and Al–40 wt% Sn; SEM and EDS microstructural analyses of Al–15 wt% Sn–NiTi and Al–40 wt% Sn–NiTi; an SEM image of the NiTi wire surface after etching and fluxing treatment; optical and SEM images of the region near the clamp before and after healing; EDS analysis of the healing agent near the clamp after healing; SEM micrographs of the crack area before and after healing in tested specimens with corresponding ImageJ analyses; and EDS elemental analysis confirming bonding of the healing agent within the crack area. See DOI: **https://doi.org/10.1039/d5ta05255f**.

Funding

This research received no external funding.

Acknowledgements

Electron microscopy, and DSC were conducted at the Advanced Analysis Facility of University of Wisconsin-Milwaukee.

References

1 S. Sharma, M. Bellah, V. Srivastava and P. Rohatgi, Gravity and Semisolid Casting of Self-Healing Aluminum Matrix Composites, *Int. J. Metalcast.*, 2025, **19**, 20–32.
2 M. Bellah, M. Nosonovsky and P. Rohatgi, in *Metal-Matrix Composites*, ed. T. S. Srivatsan, P. K. Rohatgi and S. Hunyadi Murph, Springer International Publishing, Cham, 2022, pp. 297–310.
3 M. Bellah, M. Nosonovsky and P. Rohatgi, Shape Memory Alloy Reinforced Self-Healing Metal Matrix Composites, *Appl. Sci.*, 2023, **13**, 6884.
4 P. Rohatgi, M. Bellah and V. Srivastava, Current status and future research imperatives of self-healing metal matrix composites, *J. Mater. Res.*, 2024, **39**, 1597–1621.
5 B. Grabowski and C. C. Tasan, in *Self-healing Materials*, ed. M. D. Hager, S. van der Zwaag and U. S. Schubert, Springer International Publishing, Cham, 2016, pp. 387–407.
6 M. V. Manuel and G. B. Olson, Biomimetic Self-Healing Metals, *Proceedings of the 1st International Conference on Self-Healing Materials*, 2007.
7 M. V. Manuel, PhD thesis, Northwestern University, 2007.
8 A. Concilio, V. Antonucci, F. Auricchio, L. Lecce and E. Sacco, *Shape Memory Alloy Engineering: for Aerospace, Structural, and Biomedical Applications*, Butterworth-Heinemann, 2021.
9 D. C. Lagoudas, *Shape Memory Alloys: Modeling and Engineering Applications*, SpringerScience+Business Media, LLC, New York, N.Y., 2008.
10 S. H. Zadeh, T. D. Brown, X. Qian, I. Karaman and R. Arroyave, A composition-based predictive model for the transformation strain of NiTi shape memory alloys, *Acta Mater.*, 2025, **289**, 120861.
11 M. Bellah, V. Srivastava, M. Nosonovsky, B. Church and P. Rohatgi, in *Advances in Sustainable Composites*, ed. Y. Al-Majali, B. Wisner, I. N. Mastorakos, S. E. Hunyadi Murph and M. Paramsothy, Springer Nature Switzerland, Cham, 2025, pp. 191–202.
12 N. H, S. P, N. S, M. Alsubih, S. Islam, H. S. Majdi, S. Algburi and A. Razak, Mechanical, fatigue and super plasticity properties of Cu–Al–Mn, Cu–Al–Be–Mn shape memory alloy and their metal matrix composites, *RSC Adv.*, 2024, **14**, 31275–31290.
13 K. Otsuka and X. Ren, Physical metallurgy of Ti–Ni-based shape memory alloys, *Prog. Mater. Sci.*, 2005, **50**, 511–678.
14 K. Liu, B. Yuan, T. Pan, J. Liang and Y. Gao, Microstructural origin of ultralow Lüders-like stress plateau of Nb nanowire embedded NiTi shape memory alloy, *J. Alloys Compd.*, 2025, **1032**, 181250.
15 K. Samadi-Aghdam, P. Fahimi, H. Shahsavari, D. Rahmatabadi and M. Baghani, Vibration Analysis of Shape Memory Alloy Enhanced Multi-Layered Composite

Beams with Asymmetric Material Behavior, *Materials*, 2025, **18**, 1181.
16 D. Rahmatabadi, K. Soltanmohammadi, M. Pahlavani, M. Aberoumand, E. Soleyman, I. Ghasemi, M. Baniassadi, K. Abrinia, M. Bodaghi and M. Baghani, Shape memory performance assessment of FDM 3D printed PLA-TPU composites by Box-Behnken response surface methodology, *Int. J. Adv. Manuf. Technol.*, 2023, **127**, 935–950.
17 C. R. Fisher, J. J. Mecholsky, H. B. Henderson, M. S. Kesler and M. V. Manuel, A Reactive Element Approach to Improve Fracture Healing in Metallic Systems, *Front. Mater.*, 2019, **6**, 210.
18 P. Zhu, Z. Cui, M. S. Kesler, J. A. Newman, M. V. Manuel, M. C. Wright and L. C. Brinson, Characterization and modeling of three-dimensional self-healing shape memory alloy-reinforced metal-matrix composites, *Mech. Mater.*, 2016, **103**, 1–10.
19 M. V. Manuel, in *Self-Healing Materials*, John Wiley & Sons, Ltd, 2008, pp. 251–265.
20 M. C. Wright, M. Manuel and T. Wallace, *Fatigue Resistance of Liquid-assisted Self-repairing Aluminum Alloys Reinforced with Shape Memory Alloys*, 2013.
21 C. R. Fisher, H. B. Henderson, M. S. Kesler, P. Zhu, G. E. Bean, M. C. Wright, J. A. Newman, L. C. Brinson, O. Figueroa and M. V. Manuel, Repairing large cracks and reversing fatigue damage in structural metals, *Appl. Mater. Today*, 2018, **13**, 64–68.
22 M. V. Manuel, C. R. Fisher and M. C. Wright, *US Pat.*, US10597761B2, 2020.
23 C. R. Fisher, PhD thesis, University of Florida, 2013.
24 M. A. Poormir, S. M. R. Khalili and R. Eslami-Farsani, Investigation of the Self-Healing Behavior of Sn-Bi Metal Matrix Composite Reinforced with NiTi Shape Memory Alloy Strips Under Flexural Loading, *JOM*, 2018, **70**, 806–810.
25 J. B. Ferguson, B. F. Schultz and P. K. Rohatgi, Self-Healing Metals and Metal Matrix Composites, *JOM*, 2014, **66**, 866–871.
26 V. Kilicli, X. Yan, N. Salowitz and P. K. Rohatgi, Recent Advancements in Self-Healing Metallic Materials and Self-Healing Metal Matrix Composites, *JOM*, 2018, **70**, 846–854.
27 V. Kilicli, Development of an eutectic-based self-healing in Al–Si cast alloy, *Mater. Test.*, 2022, **64**, 371–377.
28 P. Zhu, PhD thesis, Northwestern University, 2015.
29 S. K. Misra, MS thesis, The University of Wisconsin - Milwaukee, 2013.
30 N. Salowitz, S. Misra, M. I. Haider, M. Povolo and P. Rohatgi, Investigation into the Performance of NiTi Shape Memory Alloy Wire Reinforced Sn-Bi Self-Healing Metal Matrix Composite, *Materials*, 2022, **15**, 2970.
31 M. A. Poormir, S. M. R. Khalili and R. Eslami-Farsani, Optimal design of a bio-inspired self-healing metal matrix composite reinforced with NiTi shape memory alloy strips, *J. Intell. Mater. Syst. Struct.*, 2018, **29**, 3972–3982.
32 J. B. Ferguson, B. F. Schultz and P. K. Rohatgi, Zinc alloy ZA-8/shape memory alloy self-healing metal matrix composite, *Mater. Sci. Eng. A*, 2015, **620**, 85–88.
33 V. Srivastava and M. Gupta, Design and prediction of healing assessment for AA2014-Nitinol strip-Solder alloy based hybrid self-healing composite structure via Taguchi analysis and fuzzy logic approach, *Mech. Adv. Mater. Struct.*, 2022, 1–20.
34 V. Srivastava and M. Gupta, Evaluation and Prediction of Self-healing Assessments for AA2014 Based Hybrid Smart Composite Structures: A Novel Fuzzy Logic Approach, *Int. J. Eng.*, 2022, **35**, 1841–1857.
35 V. Srivastava and M. Gupta, Experimental assessment of self-healing characteristics in AA2014matrix with nitinol wire and solder alloy as healing agents, *Mater. Res. Express*, 2019, **6**, 085704.
36 V. Srivastava and M. Gupta, Experimental assessment of self-healing nature in aluminum-based smart composites with NiTi wires and solder alloy as healing agents through Taguchi approach, *J. Intell. Mater. Syst. Struct.*, 2020, **31**, 2101–2116.
37 V. Srivastava and M. Gupta, Impact of post hardening mechanism on self-healing assessment of AA2014 nitinol-based smart composites, *Met. Mater. Int.*, 2021, **27**, 2666–2681.
38 V. Srivastava and M. Gupta, Parametric assessments of self-healing characteristics in AA2014–NiTi-based metallic composites through destructive and nondestructive evaluation, *Russ. J. Nondestr. Test.*, 2020, **56**, 1064–1082.
39 V. Srivastava and M. Gupta, Approach to self healing in Metal matrix Composites: A review, *Mater. Today: Proc.*, 2018, **5**, 19703–19713.
40 S. Sharma, G. Nandan, R. Tyagi and P. Rohtagi, Fabrication, testing, and microstructural analysis of nitinol-based self-healing metal matrix composite of A356 alloy cast by semi-solid metal processing, *Adv. Mater. Process. Technol.*, 2023, 1–13.
41 S. Sharma, R. Prakash, P. K. Rohatgi and R. K. Tyagi, Rapid slurry formation technique as a possible route to produce aluminium based self- healing alloy, *Mater. Today: Proc.*, 2021, **47**, 4041–4045.
42 J. Martinez-Lucci, A. Ruzek, S. Misra, P. Rohatgi and R. Amano, Can Castings Heal Themselves?, *Mod. Cast.*, 2011, **101**, 24–27.
43 R. Amano, P. Rohatgi, J. Martínez Lucci, B. Schultz and A. Ruzek, in *7th International Energy Conversion Engineering Conference*, 2009, p. 4514.
44 J. Martinez Lucci, R. S. Amano, P. Rohatgi and B. Schultz, in *ASME International Mechanical Engineering Congress and Exposition*, 2008, vol. 48715, pp. 1759–1768.
45 J. Martínez Lucci, R. S. Amano and P. K. Rohatgi, Heat transfer and fluid flow analysis of self-healing in metallic materials, *Heat Mass Transfer*, 2017, **53**, 825–848.
46 J. Martinez-Lucci, R. S. Amano and P. Rohatgi, Review in Self Healing in Metal Matrix Composites, *J. Aeronaut. Astronaut. Aviat.*, 2021, **53**, 441–472.
47 J. Martinez Lucci, R. S. Amano, P. Rohatgi and B. Schultz, in *Energy Nanotechnology International Conference*, 2008, vol. 43239, pp. 79–88.

48 M. Taheri-Boroujeni and M. J. Ashrafi, Self-healing performance of a microcapsule-based structure reinforced with pre-strained shape memory alloy wires: 3-D FEM/XFEM modeling, *J. Intell. Mater. Syst. Struct.*, 2023, **34**(18), DOI: **10.1177/1045389X231170163**.

49 D. Svetlizky, B. Zheng, X. Wang, S. Jiang, L. Valdevit, J. M. Schoenung, E. J. Lavernia and N. Eliaz, Towards a self-healing aluminum metal matrix composite: Design, fabrication, and demonstration, *Appl. Mater. Today*, 2024, **37**, 102148.

50 M. Nosonovsky and P. K. Rohatgi, *Biomimetics in Materials Science: Self-Healing, Self-Lubricating, and Self-Cleaning Materials*, Springer, 2012th edn, 2014.

51 M. Molteni, A. M. Grande, P. Bassani and E. Gariboldi, Role of microstructure in the exploitation of self-healing potential in form-stable composite phase change materials based on immiscible alloys, *J. Alloys Compd.*, 2024, **984**, 173989.

52 J. Kim, H. J. Kim, S. H. Hong, H. J. Park, Y. S. Kim, Y. J. Hwang, Y. B. Jeong, J.-Y. Park, J. M. Park, B. Sarac, W.-M. Wang, J. Eckert and K. B. Kim, Thermally-triggered Dual In-situ Self-healing Metallic Materials, *Sci. Rep.*, 2018, **8**, 2120.

53 E. Gariboldi, M. Molteni, D. A. Vargas Vargas and K. Naumenko, Thermo-mechanical response and form-stability of a fully metallic composite phase change material: Dilatometric tests and finite element analysis, *Mater. Sci. Eng. A*, 2025, **920**, 147562.

54 L. Tanure, L. Patterer, S. Balakumar, M. Fekete, S. Mráz, S. K. Aghda, M. Hans, J. M. Schneider and H. Springer, A novel concept for self-healing metallic structural materials: Internal soldering of damage using low melting eutectics, *Mater. Des.*, 2025, **252**, 113821.

55 ASTM, *ASTM E290-09, Standard Test Methods for Bend Testing of Material for Ductility*, ASTM International, West Conshohocken, PA, USA, 2009.

56 J. I. Goldstein, D. E. Newbury, J. R. Michael, N. W. M. Ritchie, J. H. J. Scott and D. C. Joy, *Scanning Electron Microscopy and X-Ray Microanalysis*, Springer, 2017.

57 J. P. Coughlin, J. J. Williams, G. A. Crawford and N. Chawla, Interfacial Reactions in Model NiTi Shape Memory Alloy Fiber-Reinforced Sn Matrix "Smart" Composites, *Metall. Mater. Trans. A*, 2009, **40**, 176–184.

58 J. P. Coughlin, J. J. Williams and N. Chawla, Mechanical behavior of NiTi shape memory alloy fiber reinforced Sn matrix "smart" composites, *J. Mater. Sci.*, 2009, **44**, 700–707.

59 M. I. Haider, B. Church, P. Rohatgi and N. Salowitz, in *Smart Materials, Adaptive Structures and Intelligent System*, Dearborn, Michigan, USA, 2022.

60 M. I. Haider, PhD thesis, The University of Wisconsin - Milwaukee, 2023.

61 Coefficient of Thermal Expansion, **https://surfaceengineering.com/resources/coefficient-of-thermal-expansion/**, accessed 11 June 2025.

62 A. H. Committee, *Properties and Selection: Nonferrous Alloys and Special-Purpose Materials*, ASM International, 1990.

63 M. Khoshlahjeh, S. Barbarino and S. Ameduri, in *Shape Memory Alloy Engineering (Second Edition)*, ed. A. Concilio, V. Antonucci, F. Auricchio, L. Lecce and E. Sacco, Butterworth-Heinemann, Boston, 2021, pp. 591–607.

64 F. Auricchio, C. Maletta, G. Scalet and E. Sgambitterra, in *Shape Memory Alloy Engineering (Second Edition)*, ed. A. Concilio, V. Antonucci, F. Auricchio, L. Lecce and E. Sacco, Butterworth-Heinemann, Boston, 2021, pp. 195–243.

65 S. W. Robertson, A. R. Pelton and R. O. Ritchie, Mechanical fatigue and fracture of Nitinol, *Int. Mater. Rev.*, 2013, **57**, 1–37.